The Impacts of Aggregation and Surface Chemistry of Carbon Nanotubes on the Adsorption of Synthetic Organic Compounds

ARTICLE *in* ENVIRONMENTAL SCIENCE AND TECHNOLOGY · SEPTEMBER 2009

Impact Factor: 5.33 · DOI: 10.1021/es900453e · Source: PubMed

4 AUTHORS, INCLUDING:

Shujuan Zhang
Nanjing University
78 PUBLICATIONS **1,624** CITATIONS
SEE PROFILE

Sehnaz Kaplan
T.C. Süleyman Demirel Üniversitesi
14 PUBLICATIONS **347** CITATIONS
SEE PROFILE

Tanju Karanfil
Clemson University
133 PUBLICATIONS **2,597** CITATIONS
SEE PROFILE

Environ. Sci. Technol. **2009,** *43,* 5719–5725

The Impacts of Aggregation and Surface Chemistry of Carbon Nanotubes on the Adsorption of Synthetic Organic Compounds

SHUJUAN ZHANG,[†] TING SHAO,[†] S. SULE KAPLAN BEKAROGLU,[†,‡] AND TANJU KARANFIL*[,†]

Department of Environmental Engineering and Earth Sciences, Clemson University, Anderson, South Carolina 29625, Department of Environmental Engineering, Suleyman Demirel University, Isparta 32260, Turkey

Received February 12, 2009. Revised manuscript received June 9, 2009. Accepted June 11, 2009.

Effects of aggregation and surface chemistry of carbon nanotubes (CNTs) on the adsorption of three synthetic organic compounds (SOCs), phenanthrene (PNT), biphenyl (BP), and 2-phenylphenol (2PP), were investigated using commercially available pristine and surface functionalized single-walled carbon nanotubes (SWNTs), and multiwalled carbon nanotubes (MWNTs). Theoretical calculations and nitrogen adsorption analysis results demonstrated that aggregation of CNTs led to a significant reduction in surface area (especially for the SWNTs), but a significant increase of pore volume (especially for the MWNTs) due to interstices trapped in the CNT aggregates. In contrast to the nitrogen gas adsorption, the liquid phase adsorption results indicated that the adsorption of SOCs by CNTs was controlled by available adsorption surface area rather than pore volume, and aggregation of CNTs was an unfavorable factor for the SOC adsorption. Surface functionalization of CNTs improved their dispersion in aqueous solutions, but decreased their adsorption capacities for the hydrophobic SOCs, which was attributed to the formation of water clusters around the oxygen-containing functional groups. Molecular configurations of SOCs also played a role in their adsorption. For the planar PNT, the SWNTs showed significantly higher adsorption capacities and site energies than the MWNTs, whereas for the nonplanar SOCs the adsorption capacity and site energy differences between the SWNTs and the MWNTs became smaller with increasing concentration of SOCs.

Introduction

With the significant increase in the use and manufacturing of carbon nanotubes (CNTs), one major concern is the health and environmental risks posed by CNTs once they enter the environment (*1*−*3*). The nanoparticles can enter into cells, causing damage to plants, animals, and humans (*3*−*7*). In addition, due to their highly hydrophobic surfaces, CNTs exhibit strong adsorption affinities to organic chemicals, such as polycyclic aromatic hydrocarbons (PAHs) (*8*−*14*), chlorobenzenes (*15*−*17*), nitrobenzenes (*16, 18*), phenols (*19, 20*), dioxin (*21*), and natural organic matter (*14, 22, 23*). As a result, the toxicity of CNTs may be further increased by the adsorbed chemicals, and the fate and transport of toxic pollutants in the environment may be significantly altered. Therefore, understanding of organic chemical adsorption by CNTs is critical for the environmental risk assessment of both CNTs and toxic organic chemicals as well as for assessing the environmental applications of CNTs as adsorbents (*10*).

CNTs are carbon macromolecules consisting of sheets of carbon atoms covalently bonded in hexagonal arrays that seamlessly rolled into a hollow, cylindrical shape with both ends normally capped by fullerene-like tips (*25*). Based on the structure, CNTs are categorized into two main classes: single-walled carbon nanotubes (SWNTs) and multiwalled carbon nanotubes (MWNTs). SWNTs are extremely hydrophobic and prone to aggregation as bundles (Supporting Information (SI) Figure S1) due to the strong van der Waals interactions along the length axis (*26*). Aggregation is a characteristic that differentiate CNTs from other carbonaceous adsorbents (e.g., activated carbons, carbon fibers), and it may also significantly impact their adsorption properties. Aggregation leads to a reduction in the surface area (a potential negative impact for adsorption), while generating interstitial channels between nanotubes and grooves on the periphery of the nanotube bundles (a potential positive impact for adsorption). The outermost surface, inner cavities, interstitial channels, and grooves of CNTs constitute the four possible sites for adsorption (*27*). Previous studies indicate that neither CNT surface area and porosity, nor diameter alone, could be used to fully explain CNT adsorption characteristics (*9, 11, 12, 24*). Therefore, in order to understand the adsorption of organic chemicals by CNTs, their aggregation characteristics must be carefully considered in the analysis of the adsorption data. To the best of our knowledge, such analyses are rare in the literature.

To improve and control the dispersion of CNTs in water, various surface functionalization have been developed (*28*), and some functionalized CNTs have become commercially available in recent years. In addition, incidental surface functionalization can also occur during the purification procedures used to remove amorphous carbon and metal contaminants from CNTs or as a result of their exposure to oxidizing agents in the environment. Surface functionalization can change the accessibility and affinity of CNTs to adsorbate molecules. The former can be attributed to the change in the aggregation due to increase in the wettability of CNT surfaces and/or the number of available adsorption sites by either opening (removal of the end tips of CNTs by oxidation) or blocking (with functional groups or water clusters formed around the functional groups) of the inner cavities. The affinity of CNTs to adsorbate molecules is determined mainly by hydrophobic, $\pi-\pi$, H-bonding, and electrostatic interactions (*24*). The overall influence of surface functionalization on adsorption depends on the relative contribution of these individual mechanisms. Cho et al. reported that even with same surface oxide contents, the adsorption affinities of the MWNTs prepared by different oxidation methods were different (*13*). In some cases, the adsorption depended mainly on the physical aspects of the CNTs (*29, 30*), whereas in others the surface chemistry was found to play significant role in adsorption (*12, 13, 24*). Therefore, more systematic investigations are needed to better understand the adsorption behaviors of CNTs.

In the present work, we carefully examined the adsorption of three synthetic organic compounds (SOCs) by both single-

* Corresponding author phone: 1-864-656-1005; fax: 1-864-656-0672; tkaranf@clemson.edu.
[†] Clemson University.
[‡] Suleyman Demirel University.

10.1021/es900453e CCC: $40.75
Published on Web 06/25/2009

TABLE 1. Experimentally and Theoretically Obtained Characteristics of CNTs

	experimental										theoretical						
	S_{BET}	V (cm^3/g)		d_e[b]	d[c]	Length	Purity	BD[d]	O (w/w)%			d	d_e	wall	SSA (m^2/g)[f]		V (cm^3/g)	
CNT	(cm^2/g)	V_{total}	V_{HK}[a]	(nm)	(nm)	(μm)		(g/cm^3)	EA[e]	XPS	CNT	(nm)	(nm)	(−)	close-	open-	V_{inner}	V_{inter}
SWNT	486	0.722	0.031	1−2	n.d.	5−30	90+%	0.30	1.80	3.66	SWNTs	0.32	1	1	1315	2630	0.051	0.935
SWNT-OH	420	0.739	0.023	1−2	n.d.	5−30	90+%	0.30	4.08	5.41		1.32	2	1	1315	2630	0.345	0.851
SWNT-COOH	386	0.680	0.023	1−2	n.d.	5−30	90+%	0.30	3.17	4.46	MWNTs	3	9.8	10	201	263	0.046	N.A.
MWNT	164	0.664	0.060	8−15	3−5	10−50	95+%	0.05	0.00	1.53		3	13.2	15	143	175	0.024	N.A.
MWNT-OH	192	0.765	0.070	8−15	3−5	10−50	95+%	0.05	2.78	6.39		5	11.8	10	185	263	0.098	N.A.
MWNT-COOH	134	0.589	0.050	8−15	3−5	10−50	95+%	0.05	1.14	6.71		5	15.2	15	132	175	0.054	N.A.

[a] The cumulative HK pore volume of the pores smaller than 1.32 nm for SWNTs or 5 nm for MWNTs. [b] Outer diameter. [c] Inner diameter, n.d.: not determined. [d] Bulk density. [e] Elemental analysis. [f] Close- or open-ended. Diameter, length, purity, and bulk density data were provided by the manufacturers. N.A.: not available.

walled and multiwalled CNTs with a combined and in-depth analysis of CNTs' aggregation and adsorption data. By using both theoretical calculations and experimental results, we explored the impact of aggregation on the CNT surface area and pore volume, and subsequent SOC adsorption in water. The role of surface functionalization of CNTs on SOC adsorption was investigated by using commercially available CNTs because these are the types of CNTs that will be produced at large quantities and will likely to enter the environment. In addition, the role of the physicochemical properties of SOCs on their adsorption to CNTs was examined by using SOC molecules with different planarities and solubilities.

Experimental Section

Materials. Three SWNTs (pristine [SWNT], carboxyl functionalized [SWNT−COOH], and hydroxyl functionalized [SWNT−OH]) were purchased from Chengdu Organic Chemicals Co., Ltd., Chinese Academy of Sciences. Three MWNTs (pristine [MWNT], carboxyl functionalized [MWNT-COOH], and hydroxyl functionalized [MWNT−OH]) were obtained from Nanostructured & Amorphous Materials, Inc., U.S.A. CNTs were used as-received since the main focus in the study was to examine adsorption characteristics of commercially available CNTs, and one plausible scenario is that they will enter the environment without any further modification. Phenanthrene (PNT, 99.5+%), biphenyl (BP, 99+%), and 2-phenylphenol (2PP, 99+%) were obtained from Sigma-Aldrich Chemical Co. The properties of the three SOCs are summarized in SI Table S1 and their molecular configurations are schematically shown in SI Figure S2.

Characterization of CNTs. Nitrogen adsorption at 77 K and water vapor adsorption at 273 K were performed with a physisorption analyzer (Micromeritics ASAP 2010) to characterize the surface areas, pore size distributions, and surface polarity of the CNTs. The Brunauer−Emmett−Teller (BET) equation, *t*-plot method, Barret-Joyner-Halenda (BJH), and the Horvath−Kawazoe (HK) model for cylindrical pores were used to calculate surface areas, pore volumes, and pore size distributions from adsorption isotherms. Elemental analysis was performed with an EA1112 elemental analyzer (Thermo Electron Co.). X-ray photoelectron spectroscopy (XPS) analysis was performed with an XPS-KRATOS AXIS 165 spectrometer (Kratos Analytical) using a monochromatic Al K_α X-ray source (1486.6 eV). The morphologies of CNTs were observed with a transmission electron microscope (TEM, HD-2000, Hitachi, Science Systems, Ltd.) and the images are shown in SI Figure S3. The surface area and pore volume information of the six CNTs obtained from nitrogen adsorption isotherm analyses are summarized in Table 1 along with the oxygen contents obtained from elemental analysis and XPS determination and the other characterization information provided by the manufacturers.

Isotherm Experiments. Constant carbon dose aqueous phase isotherm experiments were conducted using the completely mixed batch reactors (255 mL glass bottles with Teflon-lined screw caps). Concentrated stock solutions of each adsorbate were prepared in methanol. Bottles containing about 1 mg of CNTs were first filled with distilled and deionized water (DDW) to nearly full, and then spiked with predetermined volumes of stock solution. The volume percentage of the methanol spike solution was kept below 0.1% (v/v) to minimize the cosolvent effect. No sonication was used for the isotherm experiments. The bottles with no headspace were then placed into a rotary tumbler for one week, which was found to be sufficient to reach equilibrium during preliminary kinetic experiments. After the equilibrium, the supernatants in bottles were analyzed using a high performance liquid chromatography (HPLC) analyzer at their maximum absorption and fluorescence emission wavelengths. Bottles without any adsorbent were served as blanks to monitor the loss of adsorbates during the experiment, which was found to be negligible. All experiments were performed at room temperature (20 ± 2 °C) without any buffer addition. The solution pH remained around 6.6 ± 0.3.

Isotherm Modeling. The Freundlich model was employed to analyze the isotherm data:

$$q_e = K_F C_e^n \quad (1)$$

where q_e and C_e are the equilibrated concentration of the adsorbate in sorbent and solution, respectively, K_F is a unit-capacity parameter, equal to the amount adsorbed at the value of C_e equal to unity, and n is a dimensionless parameter related to the surface heterogeneity.

The value of the K_F depends on the units used to express C_e and does not give an estimate of the effective overall adsorption capacity of the adsorbent. Therefore, a modified Freundlich equation was also employed to describe the adsorption isotherms by normalizing the C_e with the water solubility (S_w) of the adsorbate.

$$q_e = K_{F-S_w}(C_e/S_W)^n \quad (2)$$

where K_{F-S_w} is a parameter independent of the concentration units used and represents the effective overall adsorption capacity of the adsorbent. The K_{F-S_w} values are also used for comparing adsorption of organic compounds with different water solubility.

To examine energetic characteristics of sorbate/sorbent interactions, the condensation approximation was used to generate approximate energy distribution functions (*31*). With the Freundlich isotherm as a smoothing function, the approximate site energy distribution ($\phi(E)$) is described with the following function (*31*):

$$\phi(E) = \frac{K_F n S_W^n}{RT} \exp\left(\frac{-nE}{RT}\right) \quad (4)$$

where E represents the net adsorption energy calculated using the Polanyi-type potential with S_w as a reference state.

Results and Discussion

Characterization of CNTs. Both theoretical calculations and experimental analyses have been employed in this work to characterize the CNTs. By assuming that CNTs are composed of perfect sheets of carbon atoms covalently bounded in hexagonal arrays, and the MWNTs are composed of concentric walls with interwall distance as 0.34 nm, theoretical surface areas and pore volumes of the six CNTs were calculated and the results are provided in Table 1. The details of the theoretical calculations are given in the Supporting Information.

The nitrogen adsorption isotherms of each set of CNTs (pristine and surface functionalized) were of identical shape. However, the isotherms of the SWNTs and the MWNTs exhibited different adsorption patterns (SI Figure S4). The isotherms were divided into four sections, indicating multistage adsorption, and the corresponding pore sizes of the CNTs in the four relative pressure ranges were obtained by using the Kelvin equation (SI Table S2). Comparing with the diameters of the CNTs, the adsorption data in different phases suggest that less than 37 and 21% of the adsorption in the SWNT and the MWNT, respectively, were attributable to the inner cavities. The remaining adsorption volumes came from the interstitial channels and peripheral grooves formed as a result of aggregation.

The theoretical inner cavity volume (V_{inner}) in the MWNTs is small as compared to the total pore volume (V_{total}) obtained from the *t*-plot analysis of the nitrogen adsorption isotherm (Table 1). The inner cavity volume in the SWNTs with larger diameter (2 nm) occupies a considerable portion (46%) of the total volume. Therefore, for the SWNTs, the state of the nanotube ends, open or close, will significantly affect their adsorption capacity. An approach for estimating the proportion of open ends (R_{open}) in SWNTs has been established by comparing the volume of open SWNTs to its theoretical volume and by taking the purity into account (*32*). Since CNTs are cylindrical graphene sheets, the HK method based on cylindrical pore geometry was employed to calculate the pore volume. Assuming that the quantity adsorbed in pores smaller than d are all attributable to the inner cavity of open-ended SWNTs, the R_{open} was obtained by dividing the HK cumulative pore volume of the pores smaller than the upper limit of d by the theoretical inner cavity volume. The R_{open} for the SWNTs and the MWNTs were about 7−10% and 54−100%, respectively. It has been reported that surface functionalization may change the ratio of open-ended CNTs to those of close-ended (*33*). As shown by the narrow range of V_{HK} values in Table 1, the R_{open} values were hardly affected by the surface functionalization of the two CNT series used in this study.

The low R_{open} values of the SWNTs indicate that most of them were close-ended. Although the MWNTs had higher R_{open} values, the overall contribution of inner cavity volume (0.024−0.098 cm^3/g) to the total pore volume (0.589−0.765 cm^3/g) was small. Therefore, the main pore volumes of the MWNTs were located in the interstitial channels and peripheral grooves confined in the aggregated nanotubes, which agrees well with the nitrogen adsorption analysis results shown in SI Table S2. The same observation was also made for SWNTs. By using the BJH and HK equations, the pore size distributions of the SWNT and the MWNT were obtained (SI Figures S5 and S6). The MWNT had a wider pore size distribution than the SWNT. As shown in Table 1, the surface areas of the MWNTs were about $^1/_3$ of those of the SWNTs, whereas their pore volumes were relatively close to each other. However, as illustrated in SI Figure S6, the pore volume of the MWNT within the micro- and meso-pore ranges (0.35 cm^3/g) was only about half of that of the SWNT (0.64 cm^3/g). The rapid increase of pore volume of the MWNT in the macropore range demonstrated that the MWNTs formed larger interstices due to aggregation of isolated nanotubes, which was also supported by the much smaller bulk density of the MWNTs than that of the SWNTs (about $^1/_6$, Table 1).

The ratio between the experimental (S_{BET}) and theoretical specific surface areas (SSA) of the SWNTs was in the range of 0.29−0.37. Based on the established relation between the surface areas of bundled and isolated SWNTs (*34*), the above ratio suggests that the SWNT bundles were made of 2−3 layers, i.e., about 19−37 SWNTs forming a bundle with a diameter 5−7 times larger than the diameter of an isolated SWNT. As shown in Table 1, the measured V_{total} of the SWNTs was slightly lower than the calculated V_{inter}. This can be explained by the above-mentioned layered structure of the SWNT aggregates. Some of the interstices in the inner layers of the bundle, although being counted in the V_{inter}, were actually inaccessible to nitrogen molecules. The experimental SSA values of the MWNTs were very close to the theoretical data, indicating that the MWNTs were aggregated as isolated nanotubes without forming compact bundle structure as in the SWNTs. This agrees well with the TEM observation and further explains why the MWNTs had larger portion of pore volume in macropores as compared to the SWNTs. The V_{inner} values in Table 1 were obtained by assuming that all the nanotubes were open-ended. In fact, as indicated by the R_{open} values, more than 90% of the SWNTs were close-ended. Even if all the MWNTs were open-ended, the maximum V_{inner} values for the SWNTs and the MWNTs were 0.034 and 0.098 cm^3/g. Therefore, the actual contribution of the inner cavities to the total pore volume was less than 5% to the SWNTs and 20% to the MWNTs. In other words, the pore volumes of the CNTs mainly originate from the interstices trapped in the aggregates.

Although the aggregation characteristics of CNTs may change when introduced in water, the information obtained from the nitrogen adsorption isotherms provided a valuable insight into the physical structures of the CNTs in the bulk phase. In addition, water vapor adsorption and sonication−dispersion experiments were performed to evaluate the effect of surface functionalization on the affinity of water molecules to the CNT surfaces. The results showed that the surface functionalization, especially −OH, made the CNTs more polar than their pristine counterparts (SI Figures S7−S9). The low degree of water uptakes indicates that both the pristine and functionalized CNTs were highly hydrophobic, which was consistent with the aggregation behavior of CNTs observed in the isotherm bottles. After filling the bottles containing about 1 mg of CNTs with DDW, as to be used for the adsorption experiments, most of the CNTs were deposited at the bottom of the bottles (SI Figures S8−S9). Immediately after sonication for 1 h, part of the CNTs was dispersed into water, forming grayish suspensions. Analyses of CNT suspensions with visible light at 500 nm indicated that after sonication the dispersion of the MWNTs were better than that of the SWNTs, and surface functionalization with oxygen-containing functional groups exerted a positive effect on the water dispersibility of CNTs (SI Table S3).

The surface functionalization introduced more oxygen atoms on the surface of the CNTs (Table 1). The results obtained from elemental analysis (EA) reflect the composition of the bulk phase, whereas those obtained from XPS analysis are indicative of the composition on the surface within a thickness of several nanometers. The lower oxygen contents obtained from elemental analysis than those from XPS

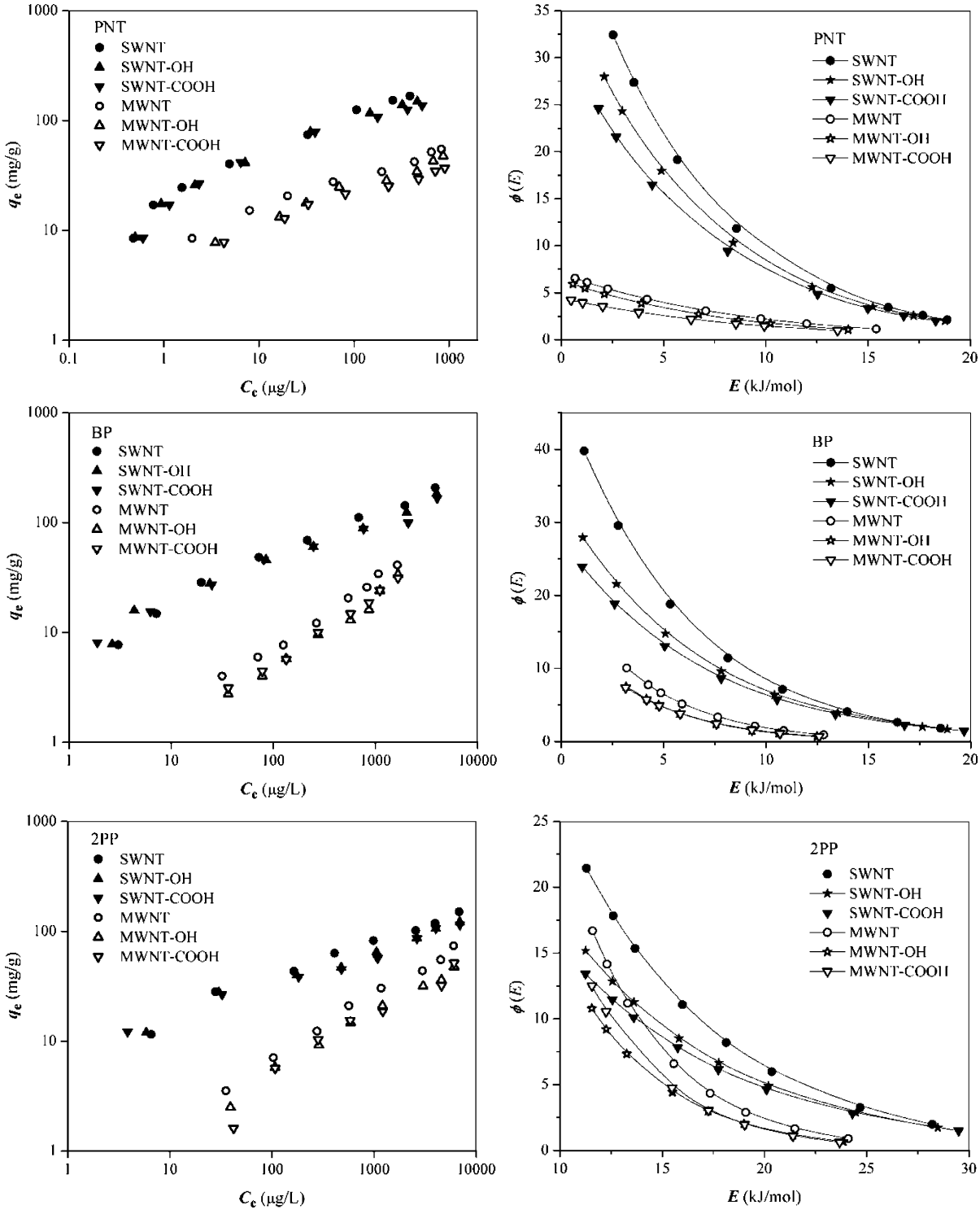

FIGURE 1. The adsorption isotherms (left panel) and adsorption site energy distribution curves (right panel) of SOCs on CNTs.

analysis indicate that the functionalization mainly occurred on the outer surface of the CNTs. Since bulk CNTs used for the measurements were in aggregate forms, the results also suggest that functional groups were directed toward the outer surfaces of the aggregates. In aqueous solutions, these surface functional groups serve as sites for water cluster formation, which may be unfavorable for the adsorption of SOCs (*35*).

Effect of CNT Structural Characteristics on Adsorption. The liquid phase adsorption isotherms of the three SOCs onto the six CNTs are illustrated in Figure 1 and their modeling parameters are summarized in Table 2. For the three SOCs, the uptakes of the SWNTs were higher than those of the MWNTs, especially at low concentrations. The specific surface area normalized adsorption capacities at saturated concentrations of SOCs (*Q* values in Table 2) showed the same trend for the planar PNT. The uptakes of the planar PNT by the SWNTs at 1 μg/L and 1 mg/L were around 3 and 5 times, respectively, to those by the MWNTs. For the nonplanar BP and 2PP, the uptake ratios of the SWNTs to the MWNTs decreased from 21 and 35 to 4 times, respectively, with increasing SOC concentration. As illustrated in Figure 1, for the planar PNT, the SWNTs showed significantly higher adsorption site energies than the MWNTs, whereas for the nonplanar SOCs the adsorption site energy difference

TABLE 2. Freundlich Isotherm Parameters of SOC Adsorption on CNTs

		K_F [(mg/g)/C_e^n][a]		n	r^2	K_{F-S_w}[b]	Q[c]	V_0	V_{total}/V_0	S_0	S_{BET}/S_0
SOC	CNT	(μg/L)	(mg/L)	(−)	(−)	(mg/g)	(mg/m^2)	(cm^3/g)	(−)	(m^2/g)	(−)
PNT	SWNT	17.20	285	0.41 ± 0.03	0.967	297	0.61	0.279	3	467	1.0
	SWNT-OH	16.55	238	0.39 ± 0.03	0.965	246	0.59	0.231	3	387	1.1
	SWNT-COOH	15.98	206	0.37 ± 0.04	0.945	213	0.55	0.200	3	335	1.2
	MWNT	7.83	58	0.29 ± 0.03	0.986	60	0.37	0.056	12	94	1.7
	MWNT-OH	5.66	48	0.31 ± 0.02	0.981	50	0.26	0.047	16	79	2.4
	MWNT-COOH	5.85	39	0.27 ± 0.02	0.977	40	0.30	0.038	16	63	2.1
BP	SWNT	6.33	125	0.43 ± 0.03	0.979	273	0.56	0.275	3	472	1.0
	SWNT-OH	7.35	104	0.38 ± 0.02	0.977	209	0.50	0.211	4	361	1.2
	SWNT-COOH	7.70	96	0.37 ± 0.02	0.981	186	0.48	0.188	4	321	1.2
	MWNT	0.45	30	0.61 ± 0.02	0.993	90	0.55	0.091	7	155	1.1
	MWNT-OH	0.26	21	0.64 ± 0.03	0.985	66	0.34	0.067	11	114	1.7
	MWNT-COOH	0.33	22	0.61 ± 0.02	0.993	65	0.49	0.066	9	112	1.2
2PP	SWNT	6.75	71	0.34 ± 0.02	0.981						
	SWNT-OH	7.45	56	0.29 ± 0.01	0.981						
	SWNT-COOH	7.64	62	0.30 ± 0.02	0.984						
	MWNT	0.34	22	0.61 ± 0.02	0.990						
	MWNT-OH	0.15	16	0.67 ± 0.01	0.998						
	MWNT-COOH	0.14	16	0.69 ± 0.01	0.998						

[a] Concentration of adsorbate expressed in different units. [b] The adsorption capacities at saturated concentrations of SOCs. The isotherms of 2PP were not simulated with the solubility-normalized Freundlich model due to its high water solubility. [c] Specific surface area normalized K_{F-S_w} values.

between the SWNTs and the MWNTs became smaller with increasing concentration of SOCs. The differences in the K_F and K_{F-S_w} values of the three SOCs on the same CNT indicate that the surface areas or pore volumes of the CNTs were not the exclusive factors determining their adsorption capacities. The molecular configurations of SOCs also played a significant role in the adsorption.

The volumes occupied (V_O) by the adsorbed PNT and BP in the CNTs were calculated by dividing their effective overall adsorption capacities (K_{F-S_w}) by their densities and are summarized in Table 2. The V_O values were much lower than V_{total} determined through N_2 gas adsorption (Table 1). The surface areas occupied by the adsorbed SOCs on the CNTs (S_O) were also calculated from their K_{F-S_w} values, molecular weights, and molecular cross sections, as discussed in the Supporting Information. The S_O values were lower or comparable to the S_{BET} determined through N_2 gas adsorption. The differences in the V and S ratios were attributed to the differences in (i) packing behaviors of N_2 and SOCs in CNTs and (ii) aggregation states of the CNTs in bulk phase and in aqueous solution. Because of the relatively larger size and steric hindrance of SOCs, the surface coverage of CNTs by SOCs is smaller than that by N_2, as evidenced by the larger than 1 value of S_{BET}/S_O. In addition, in liquid solutions, water clusters are expected to form on the sites of oxygen-containing functional groups, which impede the access of SOCs to available adsorption sites. The higher S_{BET}/S_O values of surface functionalized CNTs than those of the pristine one for both PNT and BP demonstrate the presence of water cluster formation effect on the adsorption of SOCs. According to the nitrogen adsorption results, the surface areas of the MWNTs in bulk phase were close to their theoretical values, suggesting that the aggregation of the MWNTs had no significant effect on their surface areas. Since the adsorption experiments were performed without sonication, dispersion of the MWNTs into water was not expected to exert a significant effect on their aggregation structure. Compared with that in bulk phase, the bundle structure of the SWNTs in water may undergo a slight "swelling effect" due to the nanotube−water interaction. However, this swelling effect is expected to be effective only on the pore volume but not on the surface area. This has been partly demonstrated by the sonication-dispersion experiments shown in SI Figure S8. Even after sonication, most of the SWNTs still existed as compact aggregates. Since the adsorption experiments in this work were performed without sonication, the dispersion of the SWNTs into aqueous solutions was not expected to lead to any significant change in their surface areas. Therefore, similar to the adsorption by the MWNTs, the S_{BET}/S_O ratios of the SWNTs could be regarded as an index of surface coverage difference between N_2 and SOCs.

As shown in Table 2, for all the CNTs the V_{total}/V_O ratios were much higher than the S_{BET}/S_O ratios, and the V_{total}/V_O of the MWNTs were much higher than those of the SWNTs. As discussed in the characterization section, aggregation of CNTs led to a decrease of surface area but a significant increase of pore volume, especially for the MWNTs. A large portion of the nitrogen adsorption (more than 63% for the SWNTs and 79% for the MWNTs) was due to capillary condensation in meso- and macropores trapped in the aggregates. It is well-known that the adsorption behavior in mesopores does not depend only on the fluid-wall attraction, but also on the attractive interactions between fluid molecules, which may lead to the occurrence of capillary (pore) condensation (*36*). For the SOC adsorption in aqueous solutions, since the SOCs were already dissolved in the liquid phase, no capillary condensation occurred during adsorption. Therefore, most of the nanopores within the aggregates of CNTs that can be filled with N_2 could not be efficiently occupied by the SOCs. The combined analysis of S_{BET}/S_O and V_{total}/V_O ratios indicated that the adsorption of SOCs was controlled by the available adsorption surface area rather than pore volume. The increased pore volume of CNTs due to aggregation had no positive effect on the liquid phase adsorption of SOCs. Since aggregation reduces the surface areas of CNTs, it is an unfavorable factor in liquid phase adsorption. Further understanding of factors and characteristics of CNTs that impact their aggregation and thus available surface area for adsorption will be important in the investigation of CNTs' adsorption properties.

Effect of SOC Molecular Configuration on Adsorption. The $\pi-\pi$ interaction between PAH molecules and CNT surfaces is considered to be a primary factor in adsorption (*11*). The favorable adsorption states of the planar PNT and

tetracene molecules on a SWNT have been attributed to the so-called "bridge positions" (i.e., the PAH molecules aligned along the nanotube axis under an intensive $\pi-\pi$ interaction between PAH and the SWNT surface) (*11*). Since the PNT molecule is rigid, the longitudinally parallel external surface and interstitial channels of the SWNTs can provide more accessible adsorption sites for PNT than the short, entangled MWNTs. Therefore, both the Q and Freundlich n values of PNT on the SWNTs were much higher than those on the MWNTs. Contrary to PNT, the Q values of BP on the SWNTs were nearly the same as those on the MWNTs and the n values of BP and 2PP isotherms on the MWNTs were much higher than those on the SWNTs. A higher n value is indicative of a more homogeneous surface with adsorption sites being of a narrow distribution. It appears that the adsorption of the nonplanar SOCs on the MWNTs was less site-selective than that of the planar one. The possible explanation is that the nonplanar BP and 2PP are flexible and can adjust their molecular configurations to better pack in the tubular spaces of the MWNTs with diameter several times larger than their widths. The larger K_F values of PNT than those of BP and 2PP was attributed to the hydrophobic effect. After solubility-normalization, the K_{F-S_w} values of PNT were relatively comparable to those of BP.

Effect of CNT Surface Chemistry on Adsorption. As shown by the Q values listed in Table 2, surface functionalization of the CNTs led to a reduction in the adsorption of SOCs. This reduction was correlated with the oxygen-containing functional group contents on the surface of CNTs. Only a slight reduction was observed for the SWNTs, which was attributed to the small increase in the surface functional groups and surface polarity as measured with water adsorption (SI Figure S5) as a result of surface functionalization of the pristine SWNT. A 25−30% reduction in the adsorption capacity was observed at 1 mg/L of equilibrium concentration for the three SOCs on the MWNTs, which is in agreement with the 5.9% sorption capacity reduction by each additional percentage of surface oxides reported in a recent study (*13*). The main purpose of the surface functionalization of the CNTs is to improve their dispersibilities in water. The sonication-dispersion experiments confirmed this expectation, especially for the MWNTs (SI Table S3). A better dispersion of the CNTs in water will increase the available adsorption sites, which consequently can be favorable for the liquid phase adsorption. However, surface functionalization also decreases adsorption of SOCs due to water cluster formation caused by oxygen-containing functional groups on the surface or tube end of CNTs. The overall decrease in the adsorption of SOCs indicates that water cluster formation played a more important role in the adsorption of hydrophobic SOCs than the better dispersion of CNTs in water, considering also the fact that CNTs were used without any sonication in the experiments.

Acknowledgments

This work was partly supported by a research grant from the National Science Foundation (CBET 0730694). However, the manuscript has not been subjected to the peer and policy review of the agency and therefore does not necessarily reflect its views.

Supporting Information Available

Schematic structure of SWNT bundle in Figure S1, molecular configurations of SOCs in Figure S2, selected physicochemical properties if SOCs in Table S1, TEM images of CNTs in Figure S3, nitrogen adsorption isotherms of the CNTs in Figure S4, N_2 adsorption isotherm division and pore width of CNTs in Table S2, pore size distributions of CNTs in Figures S5−S6, water vapor adsorption isotherms of CNTs in Figure S7, Visible light absorbance (at 500 nm) of CNT solutions in Table S3, and the pictures of CNT dispersion and aggregation in Figures S8−S9. This material is available free of charge via the Internet at http://pubs.acs.org.

Literature Cited

(1) Colvin, V. L. The potential environmental impact of engineered nanomaterials. *Nat. Biotechnol.* **2003**, *21* (10), 1166–1170.
(2) Oberdorster, G.; Oberdorster, E.; Oberdorster, J. Nanotoxicology: An emerging discipline evolving from studies of ultrafine particles. *Environ. Health Perspect.* **2005**, *113* (7), 823–839.
(3) Wiesner, M.; Lowry, G. V.; Alvarez, P.; Dionysiou, D.; Biswas, P. Assessing the risk of manufactured nanomaterials. *Environ. Sci. Technol.* **2006**, *40* (14), 4337–4345.
(4) Jia, G.; Wanf, H.; Yan, L.; Wang, X.; Pei, R.; Yan, T.; Zhao, Y.; Guo, X. Cytotoxicity of carbon nanomaterials: single-wall nanotube, multi-wall nanotube, and fullerene. *Environ. Sci. Technol.* **2005**, *39* (5), 1378–1383.
(5) Kam, N. W. S.; Jessop, T. C.; Wender, P. A.; Dai, H. J. Nanotube molecular transporters: Internalization of carbon nanotube-protein conjugates into mammalian cells. *J. Am. Chem. Soc.* **2004**, *126* (22), 6850–6851.
(6) Lu, Q.; Moore, J. M.; Huang, G.; Mount, A. S.; Rao, A. M.; Larcom, L. L.; Ke, P. C. RNA polymer translocation with single-walled carbon nanotubes. *Nano Lett.* **2004**, *4* (12), 2473–2477.
(7) Foley, S.; Crowley, C.; Smaihi, M.; Bonfil, C.; Erlanger, B. F.; Seta, P.; Larroque, C. Cellular localization of a water-soluble fullerene derivative. *Biochem. Biophys. Res. Commun.* **2002**, *294* (1), 116–119.
(8) Gotovac, S.; Hattori, Y.; Noguchi, D.; Miyamoto, J.-I.; Kanamaru, M.; Utsumi, S.; Kanoh, H.; Kaneko, K. Phenanthrene adsorption from solution on single wall carbon nanotubes. *J. Phys. Chem. B* **2006**, *110* (33), 16219–16224.
(9) Yang, K.; Zhu, L.; Xing, B. Adsorption of polycyclic aromatic hydrocarbons by carbon nanomaterials. *Environ. Sci. Technol.* **2006**, *40* (6), 1855–1861.
(10) Yang, K.; Wang, X.; Zhu, L.; Xing, B. Competitive sorption of pyrene, phenanthrene, and naphthalene on multiwalled carbon nanotubes. *Environ. Sci. Technol.* **2006**, *40* (18), 5804–5810.
(11) Gotovac, S.; Honda, H.; Hattori, Y.; Takahashi, K.; Kanoh, H.; Kaneko, K. Effect of nanoscale curvature of single-Walled Carbon Nanotubes on Adsorption of Polycyclic Aromatic Hydrocarbons. *Nano Lett.* **2007**, *7* (3), 583–587.
(12) Gotovac, S.; Yang, C. M.; Hattori, Y.; Takahashi, K.; Kanoh, H.; Kaneko, K. Adsorption of polyaromatic hydrocarbons on single wall carbon nanotubes of different functionalities and diameters. *J. Colloid Interface Sci.* **2007**, *314* (1), 18–24.
(13) Cho, H. -H.; Smith, B. A.; Wnuk, J. D.; Fairbrother, D. H.; Ball, W. P. Influence of surface oxides on the adsorption of naphthalene onto multiwalled carbon nanotubes. *Environ. Sci. Technol.* **2008**, *42* (8), 2899–2905.
(14) Wang, X. L.; Lu, J. L.; Xing, B. S. Sorption of organic contaminants by carbon nanotubes: Influence of adsorbed organic matter. *Environ. Sci. Technol.* **2008**, *42* (9), 3207–3212.
(15) Peng, X.; Li, Y.; Luan, Z.; Di, Z.; Wang, H.; Tian, B.; Jia, Z. Adsorption of 1,2-dichlorobenzene from water to carbon nanotubes. *Chem. Phys. Lett.* **2003**, *376* (1−2), 154–158.
(16) Chen, W.; Duan, L.; Zhu, D. Adsorption of polar and nonpolar organic chemicals to carbon nanotubes. *Environ. Sci. Technol.* **2007**, *41* (24), 8295–8300.
(17) Fagan, S. B.; SouzaFilho, A. G.; Lima, J. O. G.; Filho, J. M.; Ferreira, O. P.; Mazali, I. O.; Alves, O. L.; Dresselhaus, M. S. 1,2-Dichlorobenzene interacting with carbon nanotubes. *Nano Lett.* **2004**, *4* (7), 1285–1288.
(18) Chen, J.; Chen, W.; Zhu, D. Adsorption of nonionic aromatic compounds to single-walled carbon nanotubes: Effects of aqueous solution chemistry. *Environ. Sci. Technol.* **2008**, *42* (19), 7225–7230.
(19) Lin, D.; Xing, B. Adsorption of phenolic compounds by carbon nanotubes: Role of aromaticity and substitution of hydroxyl groups. *Environ. Sci. Technol.* **2008**, *42* (19), 7254–7259.
(20) Yang, K.; Wu, W.; Jing, Q.; Zhu, L. Aqueous adsorption of aniline, phenol, and their substitutes by multi-walled carbon nanotubes. *Environ. Sci. Technol.* **2008**, *42* (21), 7931–7936.
(21) Long, R. Q.; Yang, R. T. Carbon nanotubes as superior sorbent for dioxin removal. *J. Am. Chem. Soc.* **2001**, *123* (9), 2058–2059.
(22) Su, F. S.; Lu, C. S. Adsorption kinetics, thermodynamics and desorption of natural dissolved organic matter by multiwalled carbon nanotubes. *J. Environ. Sci. Health A.* **2007**, *42*, 1543–1552.
(23) Hyung, H.; Kim, J.-H. Natural organic matter (NOM) adsorption to multi-walled carbon nanotubes: Effect of NOM characteristics

and water quality parameters. *Environ. Sci. Technol.* **2008**, *42* (12), 4416–4421.
(24) Pan, B.; Xing, B. S. Adsorption mechanisms of organic chemicals on carbon nanotubes. *Environ. Sci. Technol.* **2008**, *42* (24), 9005–9013.
(25) Saito, R.; Dresselhaus, D.; Dresselhaus, M. S. *Physical Properties of Carbon Nanotubes*; Imperial College Press: London, 1998, p35.
(26) Girifalco, L. A.; Hodak, M.; Lee, R. S. Carbon nanotubes, buckyballs, ropes, and a universal graphitic potential. *Phys. Rev. B* **2000**, *62* (19), 13104.
(27) Zhao, J. J.; Buldum, A.; Han, J.; Lu, J. P. Gas molecule adsorption in carbon nanotubes and nanotube bundles. *Nanotechnology* **2002**, *13* (2), 195–200.
(28) Tasis, D.; Tagmatarchis, N.; Georgakilas, V.; Prato, M. Soluble carbon nanotubes. *Chem.—Eur. J.* **2003**, *9* (17), 4000–4008.
(29) Den, W.; Liu, H.-C.; Chan, S.-F.; Kin, K. T.; Huang, C. Adsorption of phthalate esters with multiwalled carbon nanotubes and its applications. *J. Environ. Eng. Manage.* **2006**, *16* (4), 275–282.
(30) Zhao, B.; Liang, H.-D.; Han, D.-M.; Qiu, D.; Chen, S. Q. Adsorption of pyridine from aqueous solution by surface treated carbon nanotubes. *Sep. Sci. Technol.* **2007**, *42* (15), 3419–3427.
(31) Carter, M. C.; Kilduff, J. E.; Weber, W. J. Site energy distribution analysis of preloaded adsorbents. *Environ. Sci. Technol.* **1995**, *29* (7), 1773–1780.
(32) Du, W.-F.; Wilson, L.; Ripmeester, J.; Dutrisac, R.; Simard, B.; Denommee, S. Investigation of the pore structure of as-prepared and purified HiPco single-walled carbon nanotubes by N_2/Ar adsorption-implication for H_2 storage. *Nano Lett.* **2002**, *2* (4), 343–346.
(33) Zhang, J.; Zou, H. L.; Qing, Q.; Yang, Y. L.; Li, Q. W.; Liu, Z. F.; Guo, X. Y.; Du, Z. L. Effect of chemical oxidation on the structure of single-walled carbon nanotubes. *J. Phys. Chem. B* **2003**, *107* (16), 3712–3718.
(34) Peigney, A.; Laurent, C.; Flahaut, E.; Bacsa, R. R.; Rousset, A. Specific surface area of carbon nanotubes and bundles of carbon nanotubes. *Carbon* **2001**, *39* (4), 507–514.
(35) Karanfil, T.; Kilduff, J. E. Role of granular activated carbon surface chemistry on the adsorption of organic compounds. 1. Priority pollutants. *Environ. Sci. Technol.* **1999**, *33* (18), 3217–3224.
(36) Lowell, S.; Shields, J. E.; Thomas, M. A.; Thommes, M. *Characterization of Porous Solids and Powders: Surface Area, Pore Size and Density*; Kluwer Academic Publishers: Norwell, MA, 2004.

ES900453E

Supporting Information

of

The Impacts of Aggregation and Surface Chemistry of Carbon Nanotubes on the Adsorption of Synthetic Organic Compounds

Shujuan Zhang†, Ting Shao†, S. Sule Kaplan Bekaroglu†‡, Tanju Karanfil*†

†Department of Environmental Engineering and Earth Sciences
Clemson University, Anderson, SC 29625

‡Department of Environmental Engineering
Suleyman Demirel University, Isparta 32260, Turkey

*Corresponding author. tkaranf@clemson.edu, phone 1-864-656-1005, fax 1-864-656-0672

Submission: February 12, 2009

Revision: June 8, 2009

Submitted to *Environmental Science and Technology*

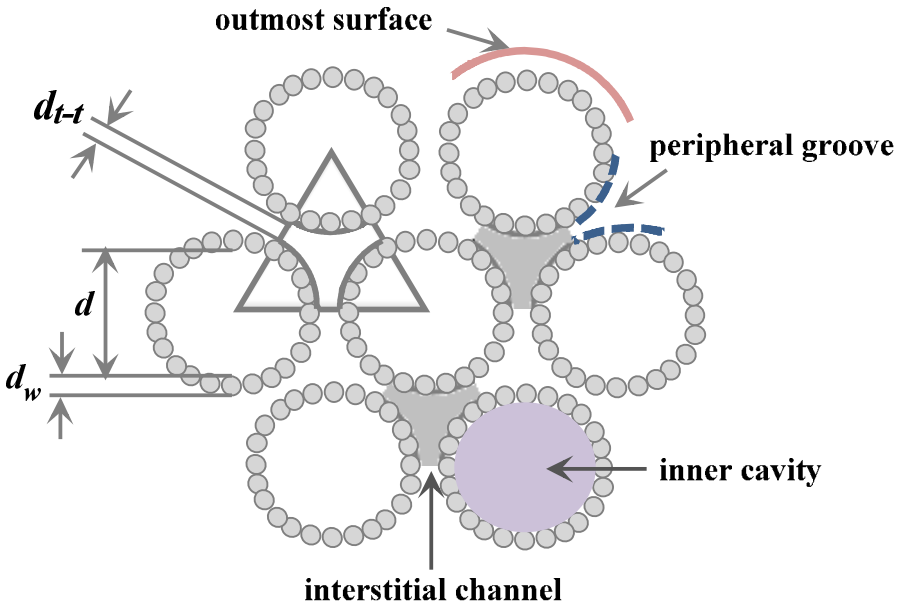

Figure S1. Schematic structure of SWNT bundle (adapted from ref. 1)

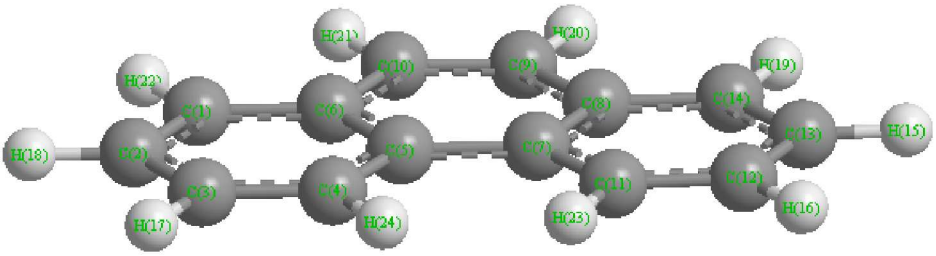

PNT

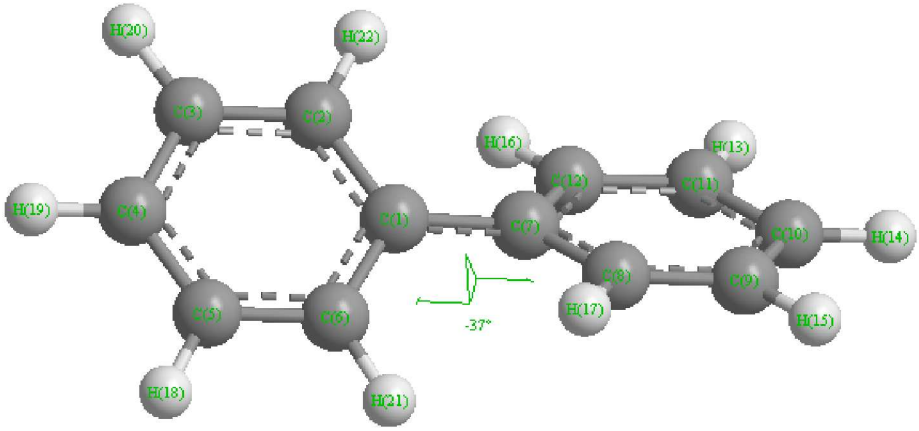

BP

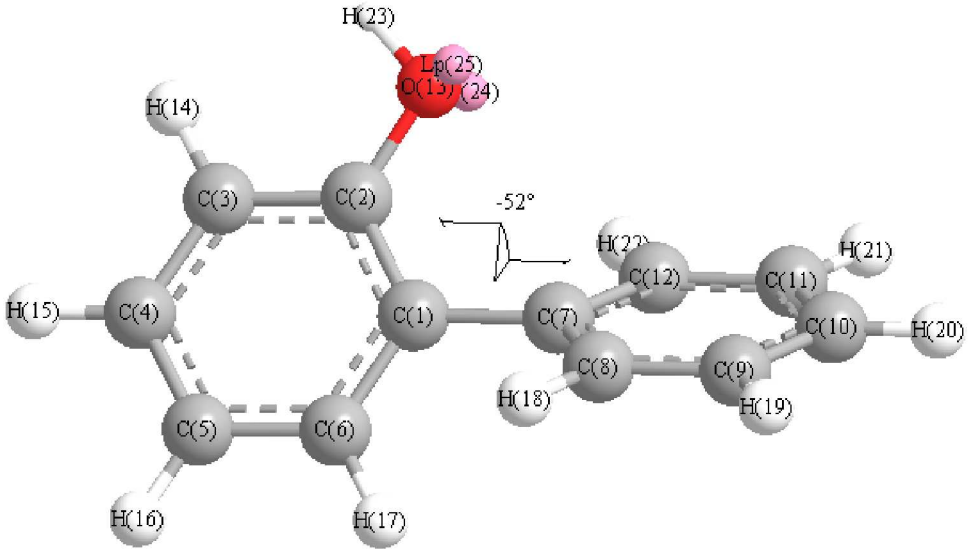

2PP

Figure S2. The molecular configuration of SOCs. (Simulated with ACDLABS 11.0)

Table S1. Selected Physicochemical Properties of SOCs

SOC	Planarity	Molecular size[a] (Å × Å × Å)	MW[b] (g/mol)	Density (g/cm^3)	MV[c] (cm^3/mol)	S_w[d] (mg/L)	pK_a	log K_{ow}[f]
PNT	Planar	11.7 × 8.0 × 3.4	178.23	1.063	167.67	1.1	n.a.	4.68 ± 0.17
BP	Nonplanar	11.8 × 6.8 × 4.7	154.21	0.992	155.45	6.1	n.a.	3.98 ± 0.23
2PP	Nonplanar	11.8 × 7.8 × 5.4	170.21	1.213	140.32	700	9.6[e]	2.94 ± 0.25

[a] Simulated with ACDLABS11.0; [b] molecular weight; [c] molecular volume; [d] water solubility; n.a.: not applicable; [e] cited from ref 2; [f] Simulated with ACDLABS11.0.

In the calculation of S_O, the molecular cross section (a_m) of SOCs on the surface of CNTs was calculated with the following equation by assuming that the packing behavior of SOCs is similar to that of nitrogen (*3*):

$$a_m = f\left(\frac{M}{\rho \cdot N_A}\right)^{2/3} \quad (1)$$

where M is the molecular weight, ρ is the density and N_A is the Avogadro constant, f is the packing factor of an adsorbate on the surface of an adsorbent. For nitrogen, f equals to 1.091.

This simple method assumes that the adsorbate forms a single layer in a pseudo-liquid packing manner. As a matter of fact, the packing behaviors of adsorbates may vary. In addition, for the SOCs, due to the large molecular size and heterogeneity in the three dimensions, the packing density might be much lower than that of nitrogen.

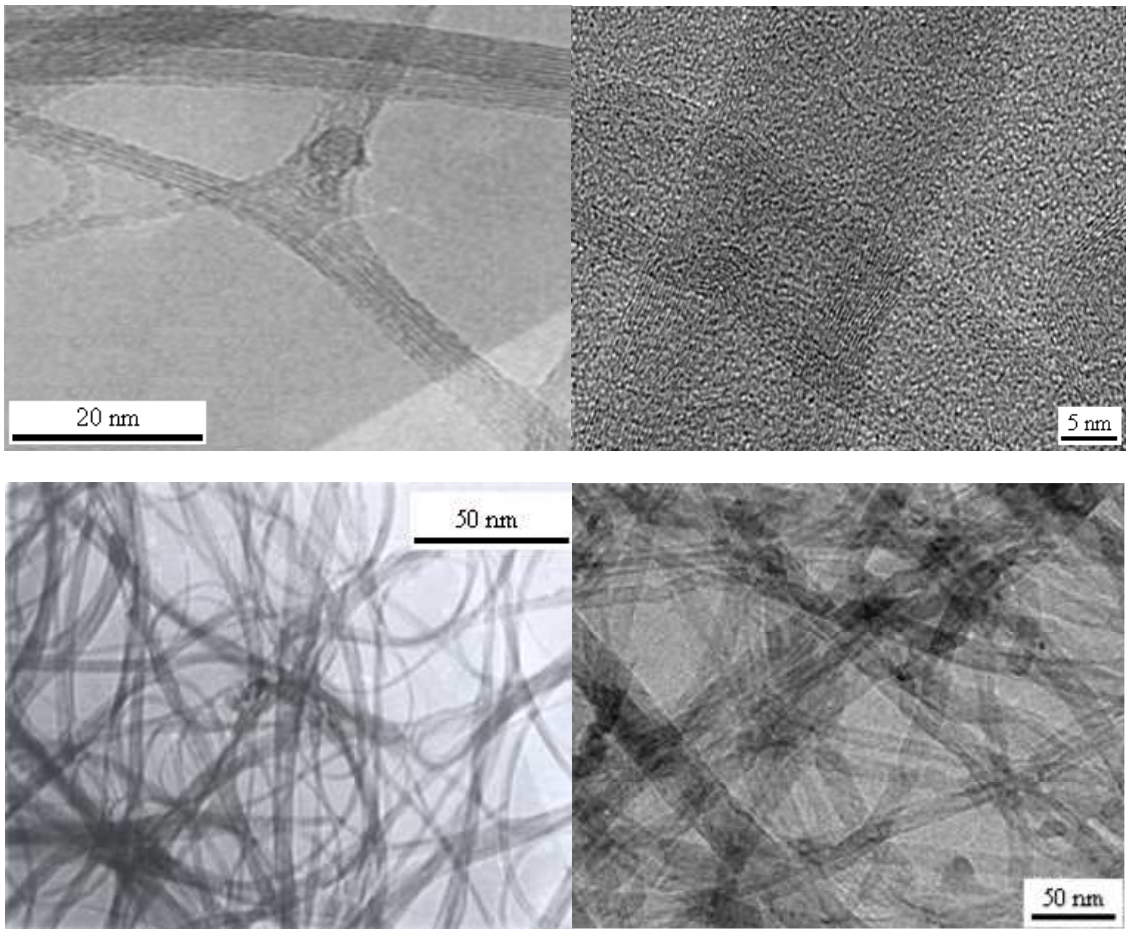

Figure S3. TEM images of the SWNT (left, from the manufacturer) and the MWNT (right).

Theoretical Calculation of the Specific Surface Area (*SSA*) and Pore Volume (*V*) of CNTs

The calculations of *SSA* are adopted from a previous report (*4*) and all calculations are based on the following hypotheses: (1) the length of the C-C bonds in the curved graphene sheets is the same as in the planar sheet, (i.e. $d_{C\text{-}C}$ = 0.1421 nm), (2) the MWNTs are composed of concentric walls and the inter-wall distance is $d_{w\text{-}w}$ = 0.34 nm, (3) the aspect ratio of CNTs is sufficiently high to neglect the area and volume of the tip ends.

In the graphene sheet, two carbon atoms occupy a surface area of one hexagon ($S_{C\text{-}C}$):

$$S_h = 3{d_{C-C}}^2 \sin(\theta) = 5.2461 \times 10^{-2}\ \text{nm}^2 \quad (1)$$

where 2θ equals to the angle of the hexagon, i.e. 120°.

One gram of carbon composes the following number of hexagon (N_h)

$$N_h = N/2M_C = 2.5075 \times 10^{22}\text{g}^{-1} \quad (2)$$

where M_C is the molecular weight of C (12.01 g/mol) and N is the Avogadro number (6.023×10^{23} mol^{-1}).

Thus, the *SSA* of one side of a graphene sheet (SSA_G) is

$$SSA_G = S_h N_h \times 10^{-18} = 1315\ \text{m}^2/\text{g} \quad (3)$$

Providing that all the ends of SWNTs are closed, the *SSA* of the SWNTs (SSA_S) should be 1315 m^2/g. Otherwise, the maximum SSA_S will be 2630 m^2/g.

The theoretical surface areas of MWNTs depend on the number of walls and the diameter. For a MWNT with an inner diameter of d and the number of walls as m, the length of the nanotube composed by one gram of carbon (L) is

$$L = \frac{N_h L_l}{\frac{\pi\left[m(d+d_W)+2d_{W-W}\sum_{i=1}^{m-1} i\right]}{L_p} - 2n} \quad (4)$$

where d_w is the wall thickness of the nanotube, L_p is the length of one hexagon in the radial direction and L_l is the length of one hexagon in the axile direction, i is the sequence number of the walls. The product of L_p and L_l is namely S_h.

To date, the exact value of d_w is still a controversial issue. Some studies assumed that d_w changes with tube diameter and is proportional to the curvature of the tube wall, ranging from 0.06 to 0.09 nm, whereas others considered that d_w is equal to d_{w-w}, i.e. 0.34 nm (*5, 6*). According to the TEM images reported in the literature and our own observation (Figure S3), 0.34 nm seems more reasonable for the CNTs. Therefore, in the present work, 0.34 nm was employed as the value of d_w.

The second term in the denominator of equation 4 is the number of C atoms that repeatedly counted in one radial unit. Since the aspect ratio of CNTs is sufficiently high, this term is negligible. As a result, the equation can be simplified to:

$$L = \frac{N_h S_h}{\pi\left[m(d+d_w)+2d_{w-w}\sum_{i=1}^{m-1} i\right]} = \frac{SSA_G \times 10^{18}}{\pi\left[m(d+d_w)+2d_{w-w}\sum_{i=1}^{m-1} i\right]} \quad (5)$$

If the ends of MWNTs are closed, the *SSA* of the MWNTs (SSA_M) depends on the diameter of the outermost graphene layer, i.e.,

$$SSA_M(\text{close}-\text{ended}) = \pi(d+2md_{w-w})L \times 10^{-18}$$

$$= \frac{(d+2md_{w-w})}{m(d+d_w)+2d_{w-w}\sum_{i=1}^{m-1} i} SSA_G \quad (6)$$

However, if the ends of MWNTs are open, since the inter-wall cavities between the concentric shells of MWNTs are inaccessible to most molecules, the SSA_M depends on the outermost and the innermost diameter of the nanotubes.

$$SSA_M(\text{open}-\text{ended}) = \frac{2(d+md_{w-w})}{m(d+d_w)+2d_{w-w}\sum_{i=1}^{m-1} i} SSA_G \quad (7)$$

The pore volume of CNTs comes from two parts: one is the inner cavities of the nanotubes if at least one end of the nanotube is opened or if there are nano-windows in the outer surface. Another part is the interstices that generated by the aggregation of nanotubes. The volume of the inner cavity (V_{inner}) is determined by the innermost diameter of the CNTs:

$$V_{SI} = \pi(d/2)^2 \frac{N_h L_l}{\pi(d+d_w)/L_p} \times 10^{-21} = \frac{d^2}{4(d+d_w)} SSA_G \times 10^{-3} \text{cm}^3/\text{g} \quad (8)$$

$$V_{MI} = \pi(d/2)^2 L \times 10^{-21} = \frac{d^2}{4\left[m(d+d_w)+2d_{w-w}\sum_{i=1}^{m-1} i\right]} SSA_G \times 10^{-3} \text{ cm}^3/\text{g} \quad (9)$$

TEM images have shown that SWNTs adhere to each other and form bundles or ropes due to strong van der Waals interaction forces along the length axis, whereas MWNTs tangles randomly. The formation of bundles leads to a reduction of accessible surface area and an increase of pore volume. Since the aggregation of MWNTs is in a random way, changes in the surface area and pore volume of MWNTs are not expected. On the other hand, the surface area reduction in SWNTs caused by bundling has been discussed in detail (*4*). Because of the formation of bundles (Figure S3), the pore volume of SWNTs is determined by the entire bundle instead of an individual nanotube. Assuming that every three nanotubes are perfectly arranged in a triangular network and that the distance between two adjacent SWNTs ($d_{t\text{-}t}$) equals to $d_{w\text{-}w}$ = 0.34 nm (Figure S1), the volume ratio (R_v) of the interstices (V_{inter}) to the inner cavities of the SWNTs (V_{SI}) is:

$$R_V = \frac{V_{inter}}{V_{SI}} = \frac{(d+2d_w+d_{t-t})^2 \sin(\theta) - \pi(d/2)^2}{\pi(d/2)^2} \quad (10)$$

Thus, the volume of the interstices in SWNTs can be estimated by the inner cavity volume. By virtue of the given parameters of CNTs and the equations above, the theoretical surface areas and pore volumes of the six CNTs used in this study were calculated, and the results are summarized in Table 1.

Analysis of the nitrogen adsorption isotherms of CNTs

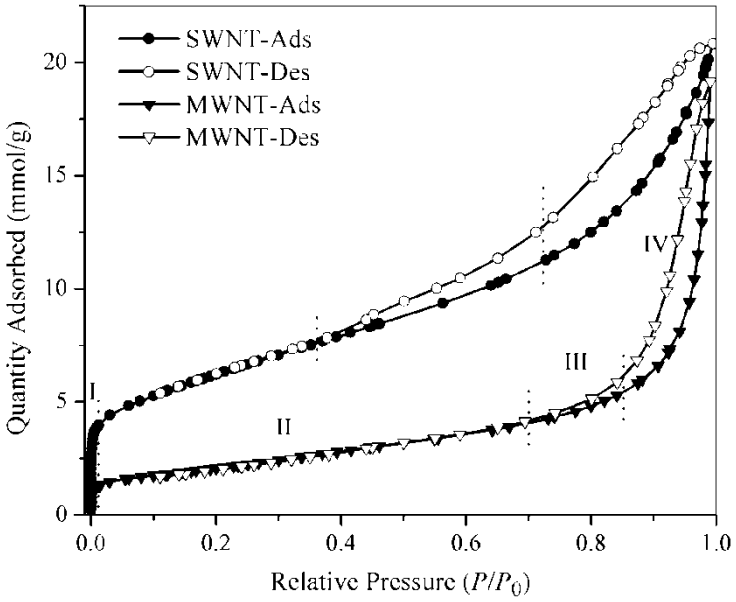

Figure S4. Nitrogen adsorption isotherms of the SWNT and the MWNT.

The nitrogen adsorption isotherms of both the SWNT and the MWNT can be divided into four sections, indicative of multi-stage adsorption. At ultra-low pressures (Phase I), the adsorption increased rapidly. Since the thermal transition hard-sphere diameter of the nitrogen molecule was 0.386 nm, such an adsorption process indicates the presence of micropores that contributed by open inner cavities or some interstices in the CNTs with diameters larger than 0.386 nm. The next section of the isotherms (Phase II) showed a surface adsorption process, in which the nitrogen adsorption increased slowly and linearly. Hysteresis loops existed in the isotherms of both the SWNTs and the MWNTs, which were associated with capillary condensation in meso- and macro-pores. However, the hysteresis loop in the isotherm of the SWNT was different from that of the MWNT. For the MWNT, it can be clearly divided into two parts: a slow capillary condensation at the medium relative pressure (Phase III) and a sharply increased capillary condensation at the high pressure range (Phase IV). Such a division was not apparent for the

SWNT and the nitrogen adsorption gradually increased. The four phases in the nitrogen adsorption isotherms of the CNTs can be attributed to micropore filling, monolayer formation, capillary condensation in mesopores and macropores, respectively.

According to the Kelvin equation, the radius of the adsorbed liquid droplet can be obtained from the relative pressure (P/P_0).

$$ln\frac{P}{P_0} = -\frac{2\gamma V_L}{RT}\cdot\frac{1}{r_m} \quad (14)$$

where γ is the surface tension of the adsorbate molecule, V_L is the molar volume of the liquid adsorbate, and r_m is the radius of the droplet.

For liquid nitrogen, the γ, V_L and T were 8.72 mN/m, 34.68 cm^3/mol, and 77.4 K, respectively (*3*). The statistic thickness of adsorbed nitrogen layer (t) can be calculated with the following equation:

$$t = (v/v_m)\cdot\sigma \quad (6)$$

where v and v_m are the adsorbed quantity at a relative pressure and the single-layer adsorbed quantity, $\sigma = 0.354$ nm is the thickness of a single liquid nitrogen layer.

As a sum of r_m and t, the corresponding pore sizes of the CNTs in the four relative pressure ranges were obtained and are summarized in Table S2.

Table S2. Adsorption isotherm division and pore size distributions of CNTs

	SWNT				MWNT			
Phase	P/P_0	Pore width (nm)	Q_{ads} [a] (mmol/g)	Ads% [b]	P/P_0	Pore width (nm)	Q_{ads} (mmol/g)	Ads%
I	0.01	0.57	3.9	19	0.01	0.85	1.3	7
II	0.36	1.63	7.6	18	0.70	4.64	4.0	14
III	0.72	3.90	11.2	17	0.85	8.48	5.4	7

IV	0.99	95.47	20.8	46	0.99	103.10	19.1	72

[a] Quantity adsorbed; [b] The adsorption percentage in each pressure range.

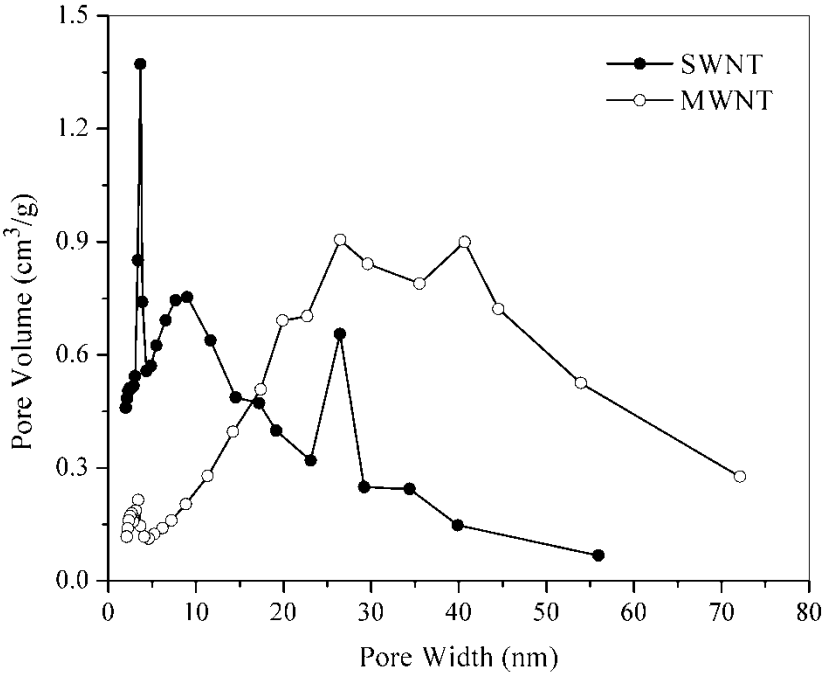

Figure S5. BJH desorption pore size distribution curves of the CNTs.

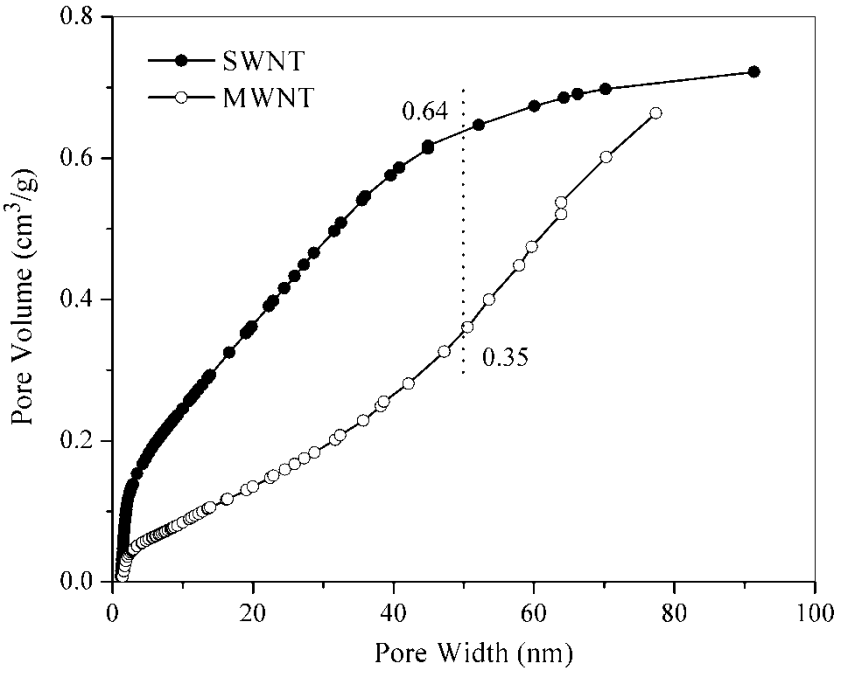

Figure S6. HK cumulative pore size distribution curves of the CNTs.

Water vapor adsorption and sonication-dispersion experiments

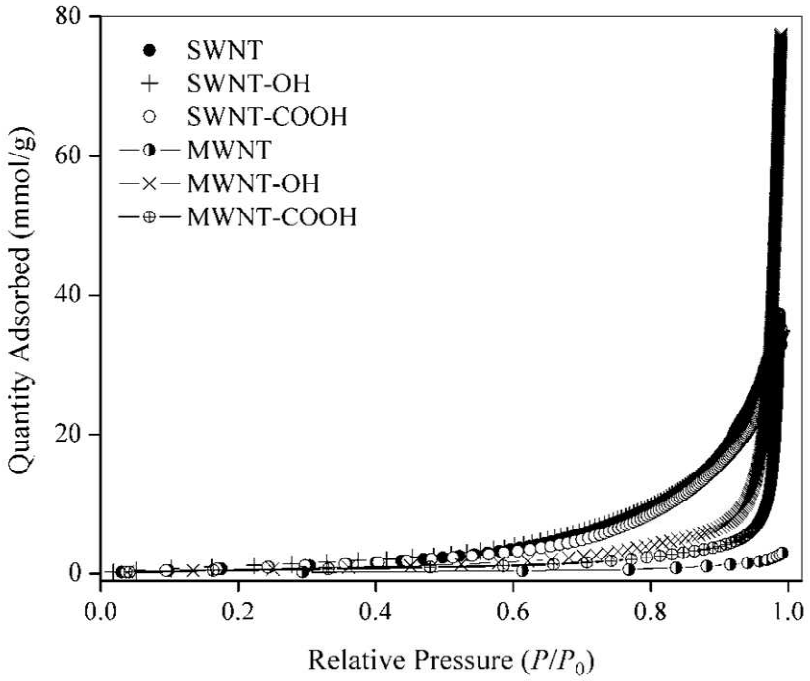

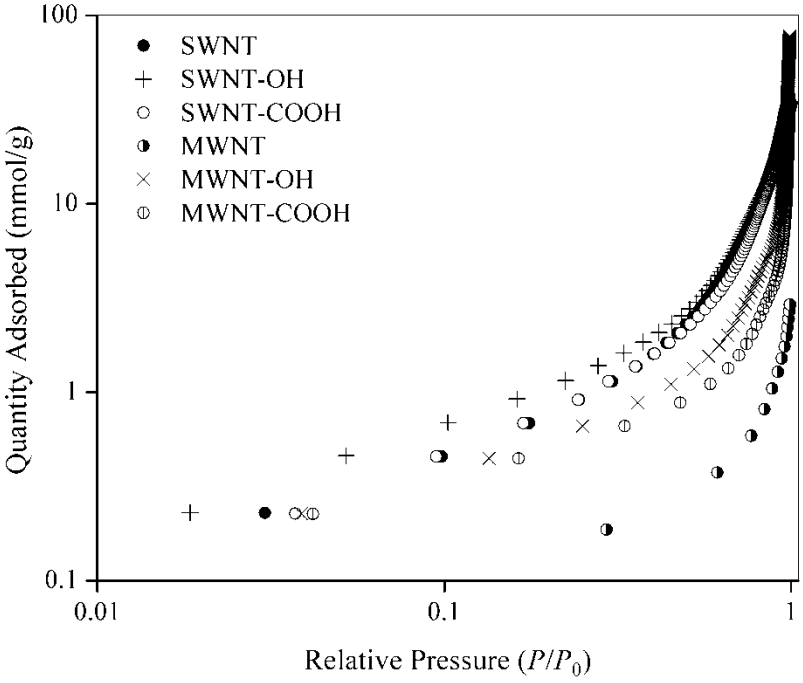

Figure S7. Water vapor adsorption isotherms of CNTs in linear (upper) and log-scale (lower) axes.

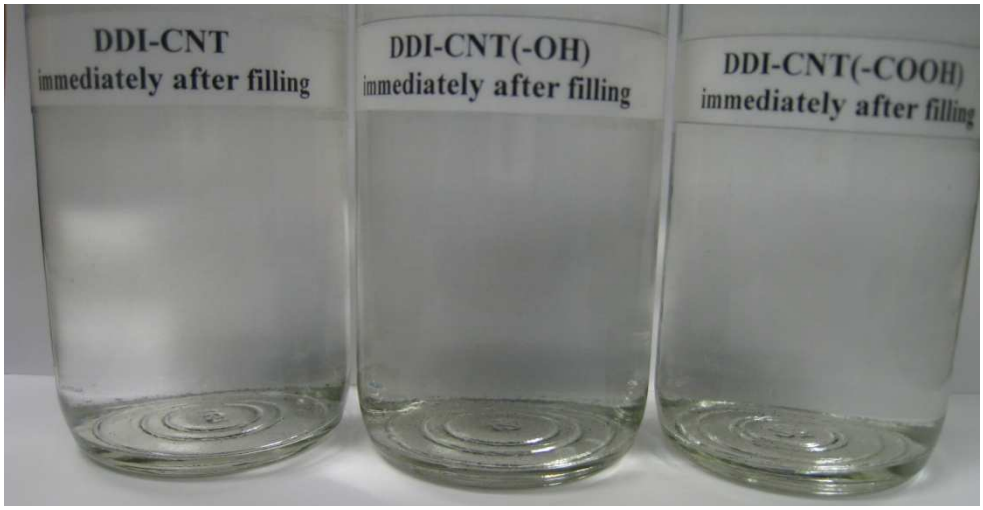

Figure S8. The aggregation status of the SWNTs in water.

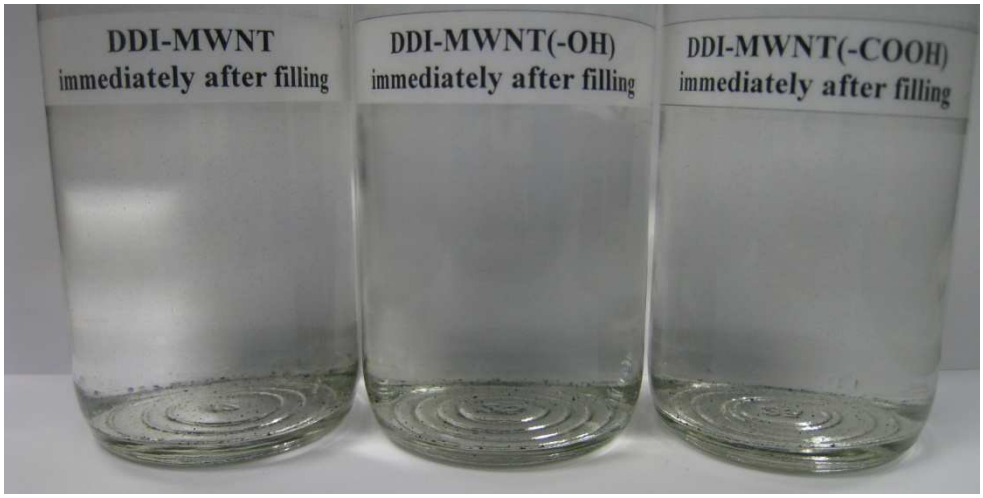

Figure S9. The aggregation status of the MWNTs in water.

Table S3. Visible light absorbance (at 500 nm and 5 cm cuvette) of CNT solutions before and after sonication for 1 h

Sonication	SWNT	SWNT-OH	SWNT-COOH	MWNT	MWNT-OH	MWNT-COOH
Before	0.003	0.004	0.002	0.006	0.002	0.001
After	0.109	0.191	0.120	0.218	0.486	0.381

Literature Cited

1. Zhao, J. J.; Buldum, A.; Han, J.; Lu, J. P. Gas molecule adsorption in carbon nanotubes and nanotube bundles. *Nanotech.* **2002,** *13* (2), 195-200.
2. Aynur O. Aptula et al., Multivariate discrimination between modes of toxic action of phenols. *Quant. Struct.-Act. Relat.* **2002**, *21*(1), 12-22.

3. Gregg, S. J.; Sing, K. S. W. *Adsorption, surface area, and porosity*. Academic Press: London; New York, 1967.
4. Peigney, A.; Laurent, C.; Flahaut, E.; Bacsa, R. R.; Rousset, A. Specific surface area of carbon nanotubes and bundles of carbon nanotubes. *Carbon* **2001,** *39* (4), 507-514.
5. Huang, Y.; Wu, J.; Hwang, K. C. Thickness of graphene and single-wall carbon nanotubes. *Phys. Rev. B* **2006,** *74* (24), 245413.
6. Vodenitcharova, T.; Zhang, L. C. Effective wall thickness of a single-walled carbon nanotube. *Phys. Rev. B* **2003,** *68* (16), 165401.